

Headline Articles

Electrical and Structural Properties and Phase Diagram of a Molecular Superconductor β -[(CH₃)₄N][Pd(dmit)₂]₂

Akiko Kobayashi,^{*} Akihito Miyamoto,[†] Reizo Kato,^{††} Akane Sato,^{†††} and Hayao Kobayashi^{†††}

Department of Chemistry, School of Science, The University of Tokyo, Hongo, Bunkyo-ku, Tokyo 113

[†]Matsushita Research Institute Tokyo, Inc., 3-10-1 Higashimita, Tama-ku, Kawasaki 214

^{††}Institute for Solid State Physics, The University of Tokyo, Roppongi, Minato-ku, Tokyo 106

^{†††}School of Mathematical and Physical Science, Graduate University for Advanced Studies and Institute for Molecular Science, Okazaki 444

(Received November 7, 1997)

β -[(CH₃)₄N][Pd(dmit)₂]₂ is isomorphic to [(CH₃)₄N][Ni(dmit)₂]₂, which is the first pure π acceptor molecular conductor exhibiting a superconducting transition. The crystal structure at low temperature, pressure dependence of the resistivity and the magnetic susceptibility of β -[(CH₃)₄N][Pd(dmit)₂]₂ were examined. The general features of the phase diagram of β -[(CH₃)₄N][Pd(dmit)₂]₂ resemble those of the organic superconductors. At ambient pressure, the resistivity increases gradually with lowering temperature. A superconducting transition was observed at 6–9 kbar. The highest T_c was 6.5 K. Between 5 and 6.3 kbar, a characteristic rapid resistivity decrease was observed at the small temperature range above the offset temperature of the superconducting transition. Although the resistivity is not zero, this temperature region can be regarded as a “pre-superconducting region.” Above 9 kbar the metallic state is stabilized down to low temperature. Above 5 kbar, most of the crystals exhibited resistivity anomalies around 60 K, which may be ascribed to the metal-insulator transition of the domains with α -type structure (α -[(CH₃)₄N][Pd(dmit)₂]₂), which became mixed in with the crystals of β -[(CH₃)₄N][Pd(dmit)₂]₂. The resistivity data of the highly conducting state were very noisy in the pressure range where the superconducting transition could be observed.

Since the first discovery, more than 15 years ago, of an organic superconductor, (TMTSF)₂PF₆ (TMTSF=tetramethylenetetraselenafulvalene), a vast number of molecular conductors were examined to search for new superconducting systems.¹⁾ Up to now more than 70 molecular superconductors have been developed. Among them M(dmit)₂ (M = Ni, Pd; dmit = 4,5-dimercapto-1,3-dithiole-2-thione) superconductors occupy a unique position because all the other molecular superconductors hitherto developed are the systems composed of organic π donor molecules having TTF-like skeletons.

The first molecular superconductor based on transition metal complex molecules is [TTF][Ni(dmit)₂]₂ discovered by Cassoux et al. in 1986.²⁾ This system contains the segregated columns of π donor (D: TTF) and π acceptor (A: Ni(dmit)₂) molecules. Another type of superconductor composed of D and A molecules, [EDT-TTF][Ni(dmit)₂]₂ (EDT-TTF = ethylenedithiotetrathiafulvalene) was reported in 1993 is the first ambient-pressure Ni(dmit)₂ superconductor.³⁾ Besides these DA and DA₂ types of superconductors, there

are M(dmit)₂ superconductors with closed shell cations, [R]-[M(dmit)₂]₂ [R = (CH₃)₄N⁺, (CH₃)₂(C₂H₅)₂N⁺; M = Ni, Pd], where only M(dmit)₂ molecules are responsible for the electron conduction. Therefore these systems can be regarded as the “pure π acceptor superconductors”.^{4–6)} Very recently a similar superconducting system with phosphonium cations, β' -[(CH₃)₂(C₂H₅)₂P][Pd(dmit)₂]₂ was discovered.⁷⁾

When the superconducting transition was found in the molecular system, considerable interest was concentrated in the point whether the nature of the constituent molecules is reflected in the superconducting mechanism or not. It is well known that the bond lengths of the charged molecule are slightly different from those of a neutral molecule. This means that the a_g modes of the molecular vibration can be coupled with the intermolecular electron transfer. Therefore, it might be quite natural to imagine the mechanism of the electron pair formation mediated by molecular vibrations.⁸⁾ In this picture, the stretching vibration of the central C=C double bond of TTF skeleton will be important for the electron pair formation in the organic superconductor com-

posed of TTF-like donors because of a relatively large difference in the bond length of the central C=C bonds between neutral BEDT-TTF [BEDT-TTF=bis(ethylenedithio)-tetrathiafulvalene] and BEDT-TTF cation.⁹⁾ On the other hand, the mode of the molecular vibration responsible for electron pair formation must be different in M(dmit)₂ superconductors because the central C=C bond is exchanged to M atom. In this sense, the comparison between organic superconductors and the M(dmit)₂ superconductors will be interesting. However up to now, no clear evidence has been obtained for the electron pair formation mediated by molecular vibration.

Contrary to the phonon mechanism, the importance of the spin excitation has been suggested in the typical organic superconductors such as Bechgaard salts TMTSF₂X- (TMTSF=tetramethyltetraselenafulvalene; X=PF₆, ClO₄, ...) and κ -type BEDT-TTF superconductors because the antiferromagnetic (AF) insulating phases (or spin density wave (SDW) phase) borders on the superconducting phases in these complexes.^{10–12)} Ten years ago, Fukuyama and Hasegawa have suggested that TMTSF₂PF₆ was a novel superconductor, where antiferromagnetic fluctuation plays an essential role.¹³⁾ Needless to say, SDW of TMTSF₂PF₆ state originates from the one-dimensionality of the metallic state. Despite of the large difference in the dimensionality of the electronic structures, the κ -type BEDT-TTF superconductor with two dimensional electronic structure also has an insulating phase with antiferromagnetic spin fluctuation, which neighbors on the superconducting phase.^{14,15)} It has been believed that the electron correlation is essential to realize the antiferromagnetic insulating phase in κ -type BEDT-TTF system. Recently another characteristic organic conductor, λ -type BETS (=bis(ethylenedithio)tetraselenafulvalene) systems, λ -BETS₂GaBr_xCl_{4-x} ($x < 1.8$) has been discovered. The superconducting phase seems to locate near the non-magnetic insulating phase.¹⁶⁾ According to the theoretical analysis by Seo and Fukuyama, however, the insulating state of λ -BETS₂GaBr_xCl_{4-x} ($x \approx 1.0$) with the spin gap state is easily changed to the antiferromagnetic state.¹⁷⁾ Thus, there seems to be a common feature in the phase diagrams of the organic superconductors. That is, the antiferromagnetic (or SDW) insulating phase is located near the superconducting phase.

Contrary to this, it has been reported that the charge density wave (CDW) state coexists or is in weak competition with superconducting phase in the first molecular superconductor based on transition metal complex molecules, (TTF)[Ni(dmit)₂]₂.^{18,19)} The competition between superconductivity and CDW has been also pointed out in TTF[Pd(dmit)₂]₂.¹⁸⁾ Thus, a CDW phase seems to play an essential role in the DA₂ type M(dmit)₂ superconductors. It may be interesting to examine whether this characteristic feature of the DA₂ type M(dmit)₂ superconductors can be found also in other M(dmit)₂ superconductors. In this paper, the phase diagram of the pure M(dmit)₂ superconductor β -[(CH₃)₄N]-[Pd(dmit)₂]₂ is reported.

Experimental

The black plate crystals of [(CH₃)₄N][Pd(dmit)₂]₂ were prepared electrochemically. The typical preparation condition was as follows: [(CH₃)₄N]₂[Pd(dmit)₂] was synthesized following the reported procedure.^{20,21)} 10 mg of [(CH₃)₄N]₂[Pd(dmit)₂] and 100 mg of [(CH₃)₄N]ClO₄ were dissolved in 15 ml acetone/acetonitrile (1:1) solution. Platinum wires with 1 mm diameter were used as electrodes and a constant current of 1.8 μ A was applied at 20 °C for about two weeks. The resistivities were measured by the conventional four probe method. Since the crystals were very thin plates, the resistivities were measured along the direction parallel to the plate. Four gold wires of 15 $\mu\phi$ were bonded by gold conducting paint. The high-pressure measurements were made by using a clamp-type pressure cell, where silicone oil (Idemitsu Daphne 7373) was used as pressure medium. The static magnetic susceptibility was measured by using a SQUID magnetometer down to 2 K. The low-temperature X-ray diffraction experiments were made on the Weissenberg-type low-temperature X-ray imaging plate system equipped with a helium refrigerator down to 14 K.

Results and Discussion

1. Crystal and Band Electronic Structures. As reported before,^{5,21)} [(CH₃)₄N][Pd(dmit)₂]₂ is polymorphic (α - and β -forms). α -[(CH₃)₄N][Pd(dmit)₂]₂ is a semiconductor at ambient pressure and no indication of the superconducting transition has been observed at least up to 12 kbar.²¹⁾ The β -form is isomorphous to [(CH₃)₄N][Ni(dmit)₂]₂. Since [(CH₃)₄N][Ni(dmit)₂]₂ is the first pure π acceptor conductor where superconducting behavior has been observed at high pressure,⁴⁾ the examination of the high-pressure properties of β -[(CH₃)₄N][Pd(dmit)₂]₂ is of special interest. The crystal data of β -[(CH₃)₄N][Pd(dmit)₂]₂ are: Monoclinic, C2/c, $a = 14.523(3)$, $b = 6.320(1)$, $c = 35.134(6)$ Å, $\beta = 90.94(2)^\circ$, $V = 3224.2$ Å³, $Z = 4$. As shown in Fig. 1a, the unit cell contains four tetramethylammonium cations located on twofold axes and eight Pd(dmit)₂ molecules. The Pd(dmit)₂ molecules are arranged to form diadic columns along [110] (or $\bar{1}\bar{1}0$). There are Pd(dmit)₂ conducting sheets parallel to (001), which are separated by the ammonium cations located between them. The long axes of all the Pd(dmit)₂ molecules are parallel to each other. But those in α -[(CH₃)₄N][Pd(dmit)₂]₂ take two directions alternately along a (the longest axis of the unit cell) (see Fig. 1b). In this connection, it should be pointed out that there exists a modified β -type structure (β' -type structure) in the crystals of [(CH₃)₄M][Pd(dmit)₂]₂ (M=P, As, Sb).^{21–23)} The main differences between β and β' structures are in their lattice constants β ($^\circ$) and in the orientation and position of tetrahedral anions: e.g., the lattice constants of β' -[(CH₃)₄As][Pd(dmit)₂]₂ are,²¹⁾ $a = 14.340$, $b = 6.344$, $c = 36.528$ Å, $\beta = 97.85^\circ$, space group, C2/c (the angle β is somewhat larger than that of the β -modification). The lattice constants were determined down to 14 K (see Fig. 2). The thermal expansion coefficients ($T > 100$ K) are smallest along the c direction: $\Delta a/a\Delta T = 4.3 \times 10^{-5}$, $\Delta b/b\Delta T = 2.1 \times 10^{-5}$, $\Delta c/c\Delta T = 1.1 \times 10^{-5}$ deg⁻¹. Except for the structural degree of freedom such as internal rotation, the molecules are usually considered to be rigid. Therefore

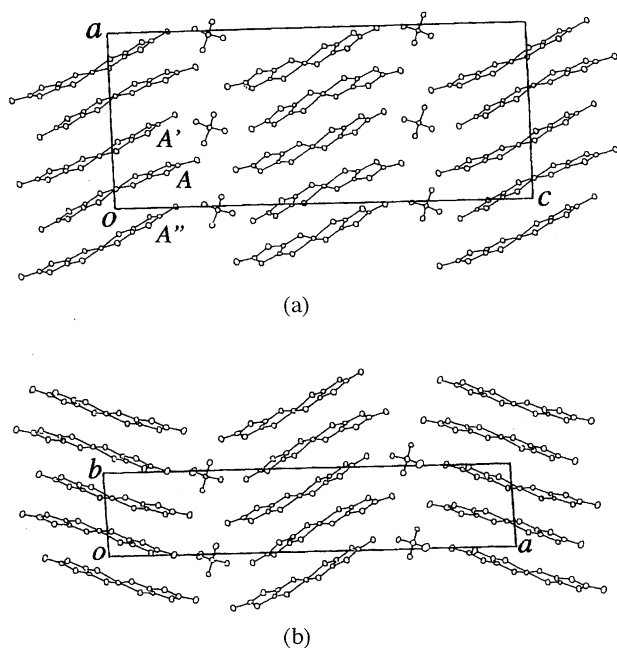


Fig. 1. (a) Crystal structure of β -[(CH₃)₄N][Pd(dmit)₂]₂. (b) Crystal structure of α -[(CH₃)₄N][Pd(dmit)₂]₂.

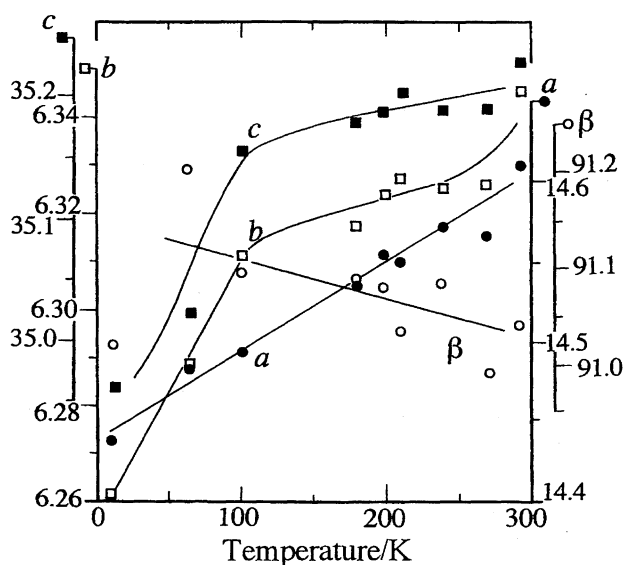


Fig. 2. Temperature dependence of the lattice constants, a , b , c Å, and β ($^\circ$) of β -[(CH₃)₄N][Pd(dmit)₂]₂.

the magnitude of thermal expansion will be determined by the thermal change of the intermolecular distances. There are four, one and four intermolecular contacts in the periodical unit along the a , b , and c directions, respectively. The average thermal expansions per one intermolecular contact between room temperature and 100 K are: $\Delta a/4 = 0.030$, $\Delta b/4 = 0.025$, $\Delta c/4 = 0.018$ Å. It was a rather unexpected result that the intermolecular contacts perpendicular to the conduction plane are more rigid than the intermolecular contacts along the conduction plane. The temperature dependencies of the lattice constants b and c become large below 100 K, but that of a was almost unchanged. The crystal structure was

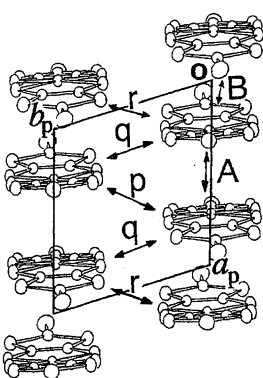
refined at 14 K. Since the crystal used for the X-ray intensity data collection was very old, the crystal seemed to be deteriorated somewhat and the reliability factor of the refinement was not satisfactory ($R = 17\%$). As reported before,²¹⁾ the Pd(dmit)₂ molecules form a dimer. The intra ($A \cdots A'$) and inter ($A \cdots A''$) dimer distances (r) are: 3.28 Å ($A \cdots A'$) and 3.82 Å ($A \cdots A''$) at R.T.; 3.26 Å ($A \cdots A'$) and 3.80 Å ($A \cdots A''$) at 14 K (see Fig. 1a). The ratio of these two interplanar distances ($r(A \cdots A')/r(A \cdots A'')$) are almost temperature-independent, which seems to be consistent with the smooth temperature change of the lattice constant a (see Fig. 2). Since Pd(dmit)₂ molecules form dimeric columns along $[110]$ (or $[\bar{1}\bar{1}0]$), there seems to be a possibility of the fourfold lattice distortion in the low temperature insulating state. In order to examine the possibility of the structural phase transition at low temperature, we took X-ray photographs down to 14 K. No significant extra reflection or diffuse scattering was observed. Therefore the possibility of CDW-like transition (or spin-Peierls transition) was ruled out at least down to 14 K.

Very recently we have made the single crystal high-pressure X-ray structure determination of the analogous Pd(dmit)₂ high-pressure superconductor, α -[(CH₃)₂(C₂H₅)₂N][Pd(dmit)₂]₂ ($T_c = 4$ K at 2.5 kbar) by using a Be-cylinder cell.²⁴⁾ The linear compressibilities of the crystal are: $\Delta a/a = 2.3 \times 10^{-3}$ kbar⁻¹, $\Delta b/b = 1.4 \times 10^{-3}$ kbar⁻¹, and $\Delta c/c = 1.6 \times 10^{-3}$ kbar⁻¹, where a ($=6.291$ Å (1 bar)), b ($=7.901$ Å (1 bar)), and c ($=18.510$ Å (1 bar)) are approximately parallel to the direction corresponding to the side-by-side arrangement of Pd(dmit)₂ molecules, the molecular stacking direction and the long axis of the molecule, respectively.²⁵⁾ It was surprising that the crystal is most compressive along the a direction, along which Pd(dmit)₂ molecules are arranged with the short intermolecular S \cdots S contacts and least compressive along the molecular stacking directions. Probably a similar change will be realized in the high-pressure state of β -[(CH₃)₄N][Pd(dmit)₂]₂. According to the well-known Grüneisen equation, the thermal expansion coefficient is roughly proportional to the compressibility. The small thermal expansion coefficients along $[001]$ and the large expansion perpendicular to it in β -[(CH₃)₄N][Pd(dmit)₂]₂ seems to be consistent with the anisotropy of the compressibility of α -[(CH₃)₂(C₂H₅)₂N][Pd(dmit)₂]₂, except for the relatively large compressibility along $[001]$ (1.6×10^{-3} kbar⁻¹), which will be related to the flexibility of ethyl groups and the positional disorder of (CH₃)₂(C₂H₅)₂N cations located on the inversion centers.

The extended Hückel tight-binding band structure was calculated based on the room temperature structure. It is well-known that, in the Pd(dmit)₂ salts with the dimeric structure, the "HOMO-LUMO energy level inversion" is realized.²⁶⁾ That is, the energy level corresponding to the state of the bonding combination of the lowest unoccupied molecular orbitals (LUMO's) of the Pd(dmit)₂ dimer becomes lower than that of the antibonding combination of the highest occupied molecular orbitals (HOMO's). The intermolecular overlap integrals of LUMO \cdots LUMO, HOMO \cdots HOMO, and

LUMO···HOMO are listed in Fig. 3. Owing to the dimeric stacks, the intradimer interaction (A(L-L) and A(H-H) (see Fig. 3)) is much larger than the others. This interaction gave the energy separation between the states of the bonding and antibonding combinations of the HOMO's or LUMO's. The energy dispersion of the extended Hückel tight-binding band is given in Fig. 4. There are four energy branches. They originate from the orbitals of bonding combination of HOMO's, bonding combination of LUMO's, anti-bonding combination of HOMO's and antibonding combination of LUMO's of two Pd(dmit)₂ molecules forming the dimer (from bottom to top (see Fig. 4)). The dimensionality of the energy bands is determined by the anisotropy of the interactions (B, p, q, r).

In the case of Ni(dmit)₂ conductors, the "HOMO-LUMO inversion" does not occur and the dimensionality of the conduction band reflects the nature of the LUMO orbital. Since the intermolecular transverse interaction is strongly diminished owing to the nodal plane of LUMO on the central transition metal atom (Ni),²⁷⁾ the band structure becomes one-dimensional (1D). Similar to Ni(dmit)₂ complexes, the transverse LUMO···LUMO interaction in the Pd system (p, q, r) is weak (see Fig. 3). But in β -[(CH₃)₄N][Pd(dmit)₂]₂, the Fermi level is on the energy branch of the anti-bonding HOMO band due to the "HOMO-LUMO inversion". The two-dimensional (2D) closed Fermi surface was obtained because of 2D HOMO···HOMO interactions (B, r, q, p).



	$S(\times 10^{-3})$		
	L-L	H-H	L-H
A	-40.7	37.6	8.8
B	2.9	7.1	2.8
p	-1.3	1.9	1.4
q	-0.8	-2.6	—
r	-0.7	5.9	2.3

Fig. 3. Intermolecular overlap integrals (S) of LUMO (L) and HOMO (H) of Pd(dmit)₂ molecules in β -[(CH₃)₄N][Pd(dmit)₂]₂.

The crystal lattice has C-centered symmetry but the primitive lattice was adopted in the calculation of the band structure. The relation of the lattice vectors of the primitive cell in the conduction plane (a_p , b_p) and the C2/c lattice (a , b) are: $a_p = (a+b)/2$, $b_p = b$.

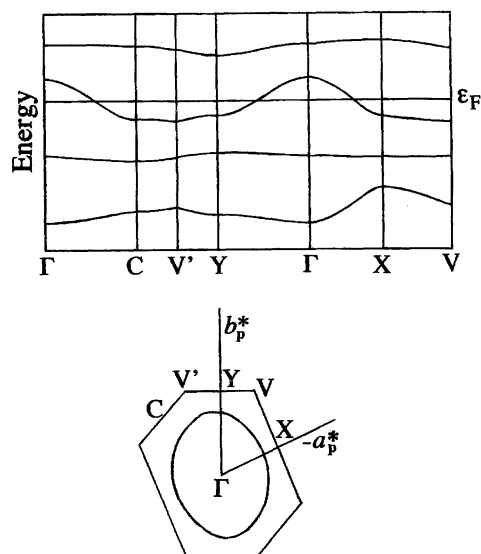


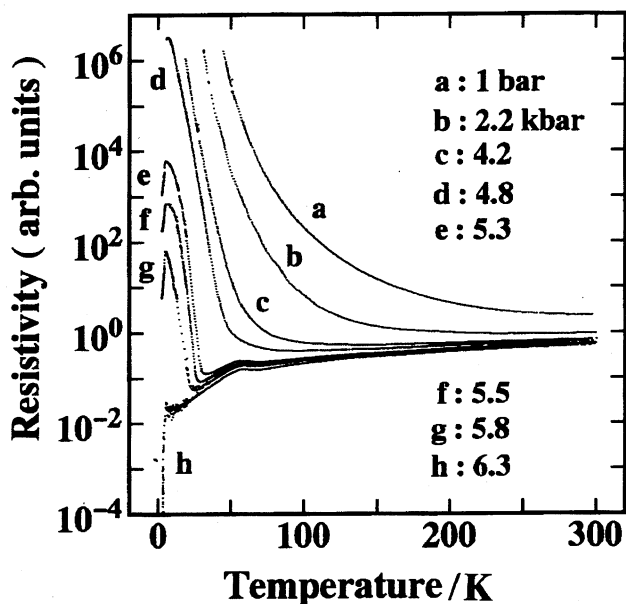
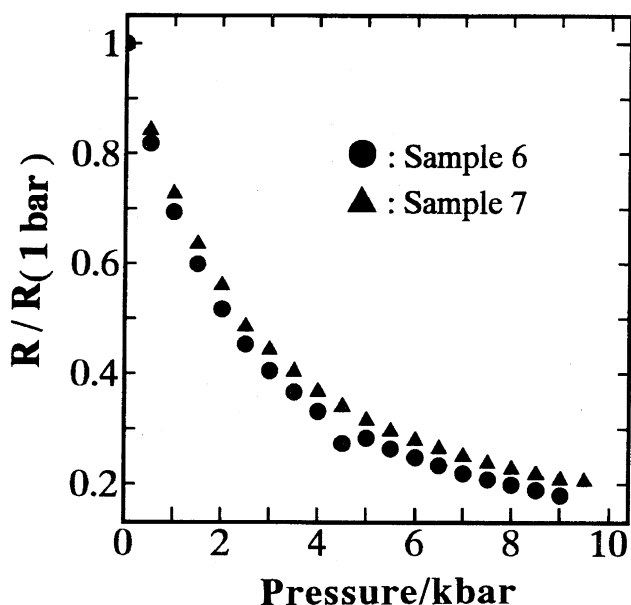
Fig. 4. Tight-binding band and the two-dimensional Fermi surface of β -[(CH₃)₄N][Pd(dmit)₂]₂.

The energy separation between the top and bottom of these four energy branches is about 1.2 eV.

Thus, the simple tight-binding band calculation indicates that the system should be a 2D metal. But as seen below, the resistivity is almost temperature independent down to 200 K at ambient pressure. The system is neither metallic nor semiconducting. This resistivity behavior resembles that of κ -type ET superconductor, κ -ET₂[Cu(N(CN)₂)]Cl (ET = bis(ethylenedithio)tetrathiafulvalene),¹¹⁾ and λ -type BETS conductors,¹⁶⁾ where the strong correlation of the conduction electrons is believed to be responsible for the non-metallic behavior in spite of the calculated 2D Fermi surfaces.

2. Resistivity Behavior. At ambient pressure, the resistivity of β -[(CH₃)₄N][Pd(dmit)₂]₂ was almost constant down to 200 K and then increased gradually (Fig. 5). The room temperature resistivity was about $3 \times 10^{-2} \Omega \text{ cm}$. The pressure dependence of the room-temperature resistivity is shown in Fig. 6. The resistivity (ρ) decreased with increasing pressure. The ratio of $\rho(10 \text{ kbar})/\rho(1 \text{ bar})$ was about 1/5. As shown in Fig. 5, the system exhibited a metallic behavior above 3 kbar. The metal-insulator (MI) transition became clear above 4 kbar and the transition temperature (T_{MI}) decreased very rapidly with increasing pressure. Around 5–6 kbar, a sharp resistivity maximum indicating a MI transition and a subsequent resistivity drop indicating the onset of superconducting transition were observed. Above 6.5 kbar, only the superconducting transition was observed. In addition, a characteristic resistivity hump was observed around 60 K. Figure 7 showed the resistivity behavior of the other sample at 6.0 kbar, where the resistivity anomaly around 60 K was also observed.

Figure 8 shows the resistivity behavior of another crystal. The superconducting transition temperature became zero at about 9 kbar, above which the system showed a normal metallic behavior. It is interesting that the "60 K anomaly" was

Fig. 5. Resistivities of β -[(CH₃)₄N][Pd(dmit)₂]₂ (Sample 1).Fig. 6. Pressure dependence of the room-temperature resistivities of β -[(CH₃)₄N][Pd(dmit)₂]₂.

absent in this crystal. A plausible origin of the sample dependence of this resistivity anomaly might be the anisotropy of the resistivity in the *ab* plane, where the magnitude of the anomaly is considered to be dependent on the direction along which the resistivities were measured. However, we have found afterwards a sample which showed a very large “60 K anomaly” (Fig. 9). The onset temperature of the “60 K anomaly” (T_0) was enhanced with increasing temperature. This behavior is reminiscent of the MI transition of α -[(CH₃)₄N][Pd(dmit)₂]₂, whose T_{MI} is enhanced at high pressure. As shown in Fig. 9b, the pressure dependence of T_{MI} of α -[(CH₃)₄N][Pd(dmit)₂]₂ closely resembles that of T_0 of β -[(CH₃)₄N][Pd(dmit)₂]₂.²¹⁾ This indicates the existence of the

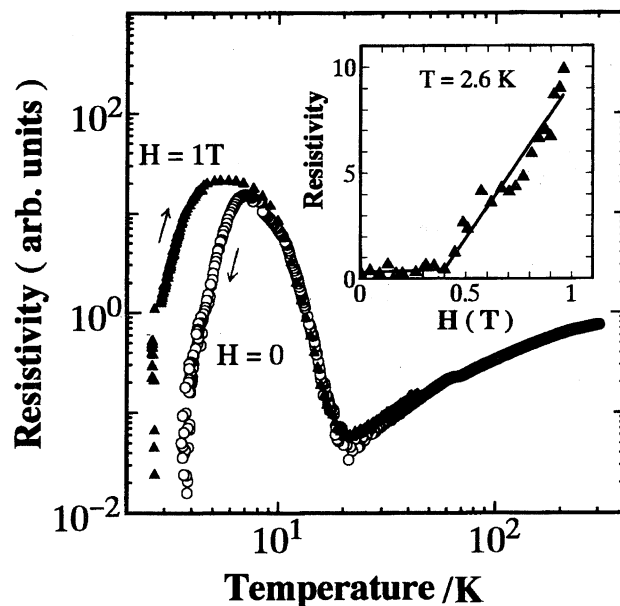
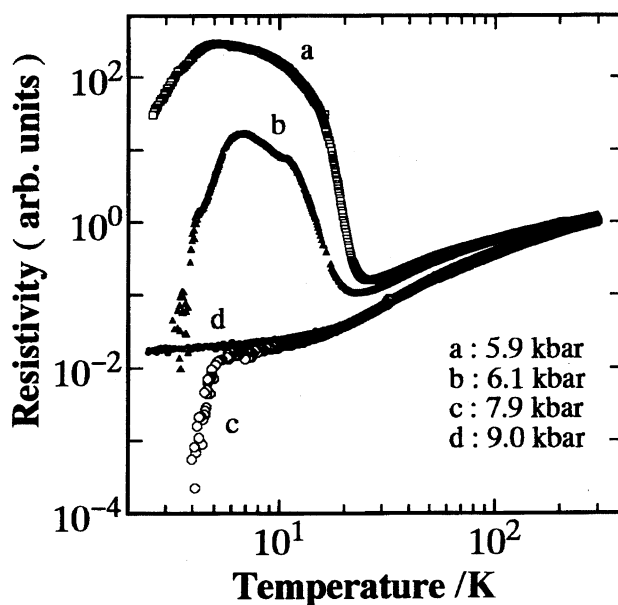
Fig. 7. Resistivity of β -[(CH₃)₄N][Pd(dmit)₂]₂ at 6.0 kbar (Sample 5). The inset is the *H*-dependence of the resistivity at 6.0 kbar and 2.6 K. The open circles indicate the resistivities at *H* = 0 and the closed triangles are those at *H* = 1 T. The arrows indicate the cooling and warming process.

Fig. 8. Pressure dependence of the resistivity of the crystal without “60 K anomaly” (Sample 7).

small domains of α -[(CH₃)₄N][Pd(dmit)₂]₂ which got mixed in with the crystal of β -[(CH₃)₄N][Pd(dmit)₂]₂. The resistivity hump around 60 K will be ascribed to the MI transition of the α -type domains. As seen from Fig. 1, the main difference between the α - and β -type structures is in the stacking sequence of the Pd(dmit)₂ layers. The alternate stacking of the Pd(dmit)₂ and ammonium layers suggests the possibility that the stacking fault will be easily formed. Another modification β' -[(CH₃)₄N][Pd(dmit)₂]₂ has not been discovered so far. Furthermore, in β' -[(CH₃)₄M][Pd(dmit)₂]₂ (M = P, As,

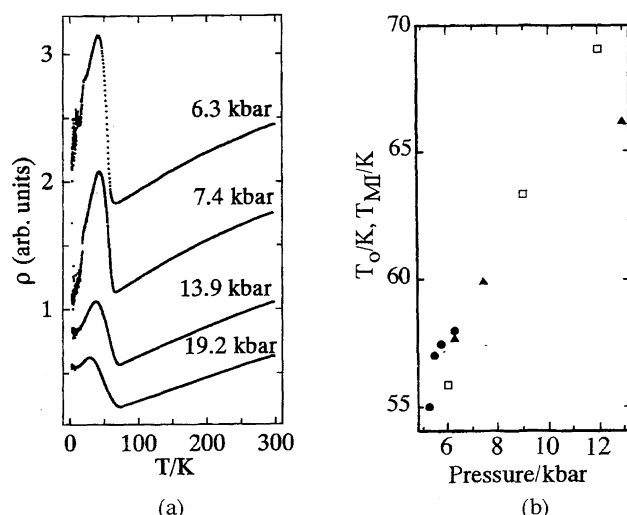


Fig. 9. (a) Resistivity behavior of the crystal exhibiting large "60 K anomaly" (Sample 10). (b) The pressure dependence of T_o (the onset temperature of the "60 K anomaly") of β -[(CH₃)₄N][Pd(dmit)₂]₂ and T_{MI} of α -[(CH₃)₄N][Pd(dmit)₂]₂. The closed circles and triangles (T_o) were obtained from the data shown in Figs. 5 and 9(a), respectively and T_{MI} (open square) was obtained from the reported data.²¹⁾

Sb), the insulating transition was suppressed with increasing pressure.^{22,23)} Therefore, the volume fraction of the domains with β' -structure will be very small even if it exists. It might be possible that a similar domain structure will be realized also in [(CH₃)₄N][Ni(dmit)₂]₂, which will afford a plausible reason why the peculiar MI transition with hysteresis and the strongly sample-dependent superconducting transition was observed in this system.²⁸⁾

3. Superconducting Transition. As shown in Fig. 5, the insulating transition was suppressed very rapidly around 4.5 kbar. But the MI transition temperature was decreased relatively slowly between 5.3 kbar and 5.8 kbar. This suggests that the nature of the insulating phase changes around 5 kbar. Between 5.3 and 6.3 kbar, the system showed a resistivity increase at 30–15 K and a subsequent sharp resistivity decrease around 6 K. When a magnetic field is applied, this resistivity drop was suppressed. A typical example of the magnetic field effect on this resistivity drop can be seen in Fig. 7. At $H=0$ T, the MI transition occurred at about 20 K and the resistivity increased very rapidly with lowering temperature and reached its maximum at 6 K, where the resistivity was about 300 times of the resistivity at 20 K. Then the resistivity dropped extremely sharply and became zero around 4 K. The sample was cooled to 2.6 K and then the magnetic field was applied parallel to the [001]. When the magnetic field was increased to 0.4 T, the resistivity was recovered (see the inset of Fig. 7). In the warming process, the resistivity was measured under the magnetic field of 1 T. The resistivity took a larger value than that of the zero-field resistivity below 7 K. Although the zero resistivity was not realized, this means that the "pre-superconducting behavior" began to develop at higher temperature (6–7 K). The exis-

tence of the "pre-superconducting temperature region" may be the most characteristic feature of this system. It should be also noted that T_{MI} is independent of the magnetic field. As seen from Figs. 5 and 7, the superconducting transition was observed at 5–9 kbar. Above 9 kbar, the system showed a metallic behavior. At 9 kbar, the temperature (T) dependence of the resistivity (ρ) is: $\rho \propto CT + \rho_0$ for $T > 80$ K, $\rho \propto C'T^{1.5} + \rho'_0$ for $25 \text{ K} < T < 60 \text{ K}$, where C (C') and ρ_0 (ρ'_0) are the constants. Below 20 K, the resistivity approached to its residual resistivity ($\rho(4 \text{ K})/\rho(300 \text{ K})=1/50$). It is remarkable that the resistivity data of the highly conducting state became very noisy at the pressure region where the superconducting transition was observed (6–9 kbar). This noisy resistivity is probably related to the superconducting phenomena of this system. Since the crystal of β -[(CH₃)₄N][Pd(dmit)₂]₂ seems to contain some small domains of α -[(CH₃)₄N][Pd(dmit)₂]₂, the inhomogeneity of the crystal is considered to disturb the electric current. With lowering temperature, the β -type domain tends to transform to the superconducting state but the insulating α -type regions located between β -type domains will terminate the conduction paths. Then the current will tend to flow through the superconducting regions formed by the connected superconducting domains and the effective current density of these regions will be increased. If the current density exceeds some critical value, the superconducting routes will be destroyed and the normal resistivity value will be recovered. This will give rise to the noisy resistivity data. Another plausible reason will be more simple. That is, the gold paint gave the insufficient contact between the gold wires (leads) and the crystals, which might cause the noisy resistivity behavior. In order to reduce the contact resistivity, four lead terminals were produced on the crystal surface by the gold deposition in the vacuum, on which the gold wires were bonded by the gold paint. But no significant change was obtained. Consequently, there seems to remain little possibility that imperfect contact is the source of the noise. At 6–7 kbar where the largest noise was observed, the noisy behavior became conspicuous below ca. 30 K. If this behavior is really related to the superconducting phenomena, some kind of superconducting fluctuation must appear around 30 K. However, the temperature of 30 K seems to be too high in comparison with the superconducting temperature of this system (<6.5 K). In this connection it might be noteworthy that the resistivity of the sample exhibiting a large "60 K anomaly" (see Fig. 9a) gave not only very noisy resistivity data but also a peculiar resistivity decrease around 20 K at 6.3 and 7.4 kbar.

The resistivity was measured with changing the magnitude of the current (Fig. 10). The cross section of the crystal perpendicular to the current was about $1 \times 0.025 \text{ mm}^2$ (sample 5). At 2.6 K, the superconducting state was maintained up to 8×10^{-4} A (ampere). On the other hand, the zero resistivity state was broken above 5×10^{-5} A at 4.2 K (current density = $2 \times 10^{-3} \text{ A mm}^{-2}$). Considering that the thin needle crystal of the organic superconductor such as λ -type BETS superconductor¹⁶⁾ with very small cross section area (e.g. 0.004 mm^2) can retain the superconducting state at least

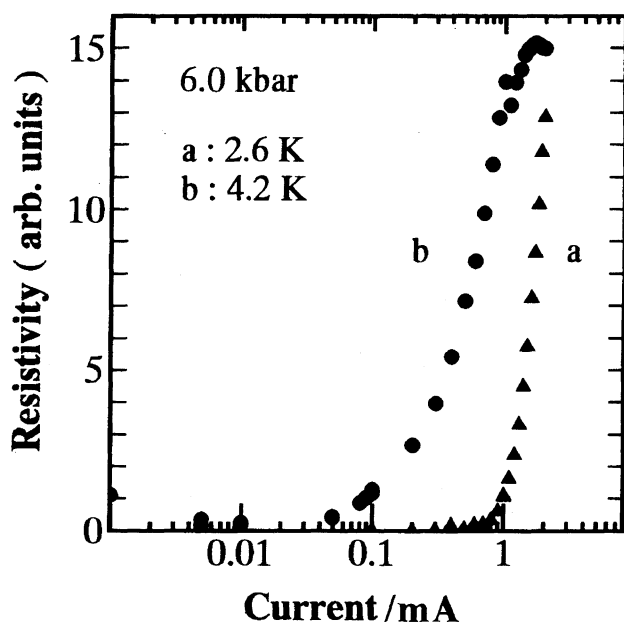


Fig. 10. The current dependence of the superconducting transition of β -[(CH₃)₄N][Pd(dmit)₂]₂ (Sample 5).

up to 1×10^{-4} A (the current density = 2.5×10^{-2} A mm⁻²), the small critical current of 5×10^{-5} A of β -[(CH₃)₄N][Pd(dmit)₂]₂ at 4.2 K suggests that the superconductivity of β -[(CH₃)₄N][Pd(dmit)₂]₂ is fragile for the large current density. This will be consistent with the domain structure model of β -[(CH₃)₄N][Pd(dmit)₂]₂.

Figure 11 shows the magnetic field effect on the resistivity at 4.2 K and 1 T. When the magnetic field was parallel to the conduction plane, the resistivity gave a sharp minimum; when the magnetic field was perpendicular to the conduction plane, a round resistivity maximum was obtained. The resistivities were dependent also on the magnitude of the current (see also Fig. 10). The current and field dependencies of the resistivity were measured up to about 6 T ($H \parallel (001)$) at 6.3 kbar (Fig. 12). The resistivity increases with increasing H and showed no indication of the saturation. But the resistivity was easily saturated when the magnetic field was perpendicular to (001) (Fig. 13). The $H_{c2\perp}$ was estimated as the mid-point of the ρ vs. H curve at 7.8 kbar (Fig. 14). The value of $|dH_{c2\perp}/dT| = 0.60$ T/K, which is more than twice the corresponding value of the ambient pressure Ni(dmit)₂ superconductor, [EDT-TTF][Ni(dmit)₂] (0.27 T/K) where the in-plane coherent length $\xi_{//}(0)$ is 310 Å.²⁹⁾ Since $dH_{c2\perp}/dT$ is proportional to $1/\xi_{//}(0)^2 T_c$, the value of $\xi_{//}(0)$ of β -[(CH₃)₄N][Pd(dmit)₂]₂ was roughly estimated as 10^2 Å.

4. Magnetic Properties. The magnetic susceptibilities of the polycrystalline samples of β -[(CH₃)₄N][Pd(dmit)₂]₂ were measured by a SQUID magnetometer in the temperature range of 2–300 K at ambient pressure. The susceptibility corrected by subtracting the calculated diamagnetic contribution is given in Fig. 15. The room-temperature susceptibility was about 4×10^{-4} emu mol⁻¹, which is almost equal to the spin susceptibility of the usual organic conductor. With de-

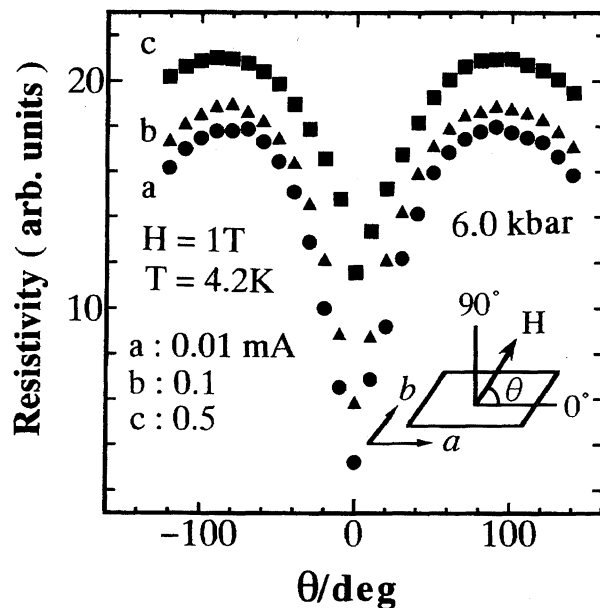


Fig. 11. Angular dependence of the magnetic field effect on the superconductivity of β -[(CH₃)₄N][Pd(dmit)₂]₂ at 6.0 kbar (Sample 7).

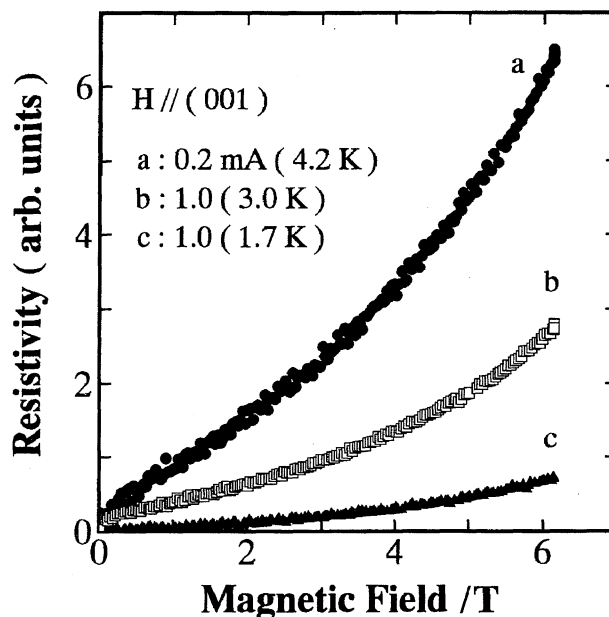


Fig. 12. Resistivity of β -[(CH₃)₄N][Pd(dmit)₂]₂ at 6.3 kbar under the magnetic field parallel to (001) (Sample 9).

creasing temperature, the susceptibility increased gradually and exhibited a round maximum around 60 K and then decreased fairly sharply down to about 20 K. The susceptibility was sample-dependent below 20 K, which will be ascribed to the lattice defects. It seemed curious that the susceptibility showed no distinct anomaly at 12 K, where a clear indication of the anti-ferromagnetic transition was detected by ¹H NMR studies.³⁰⁾ However a small anomalous peak appeared at 3 K, where a sharp change of the temperature dependence of NMR relaxation time was observed.³¹⁾ There must be some magnetic transition around 3 K. In the studies of ¹H NMR re-

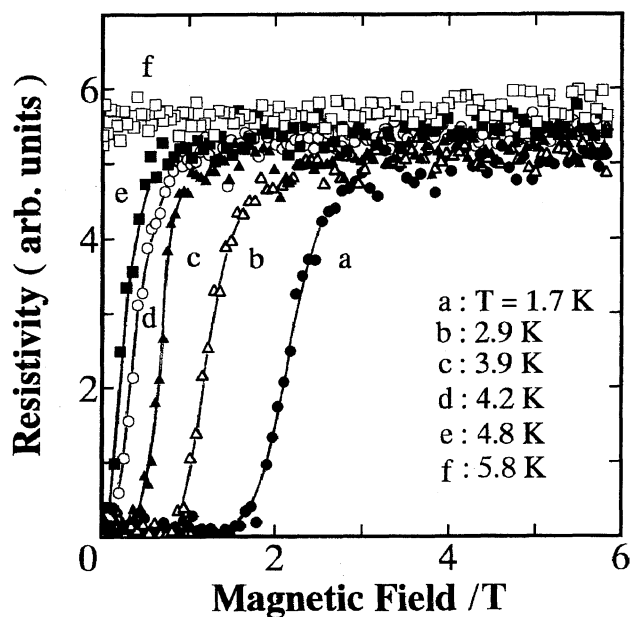


Fig. 13. Resistivity of β -[(CH₃)₄N][Pd(dmit)₂]₂ at 7.8 kbar under the magnetic field perpendicular to (001) (Sample 9).

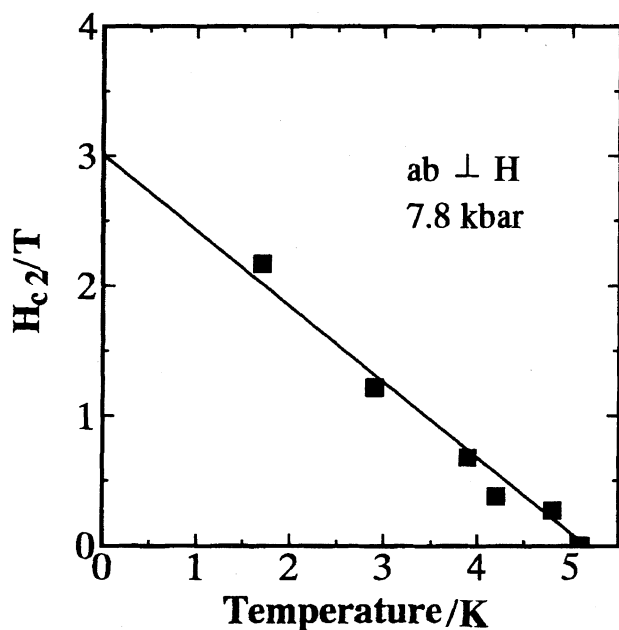


Fig. 14. The field dependence of $H_{c2\perp}$ at 7.8 kbar for the field perpendicular to (001) (Sample 9).

laxation rate, another prominent peak was observed around 120 K,³⁰⁾ which is ascribed to the reorientation motion of methyl group of (CH₃)₄N. The change of the temperature dependence of the lattice constants b and c around 100 K will be related to it (see Fig. 2). If we consider that the NMR studies disclosed the antiferromagnetic (AF) phase (or SDW) below 12 K, the decrease of the susceptibility below 60 K will be related to the development of the AF fluctuation. A similar susceptibility decrease around 60 K was also observed in κ -ET₂Cu[N(CN)₂X] (X = Cl, Br), where the AF fluctuation is believed to develop at the same temperature

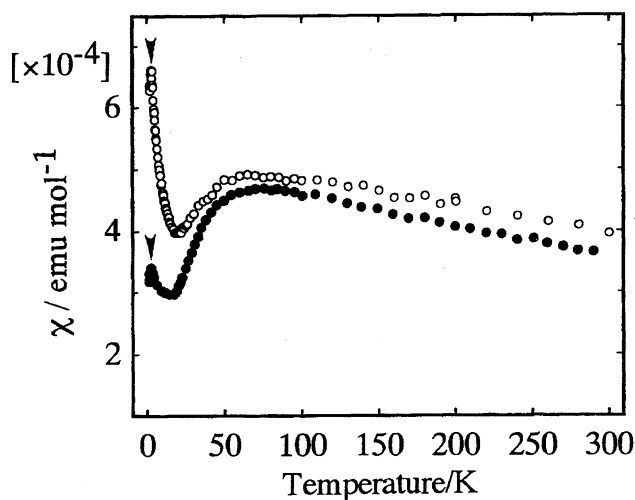


Fig. 15. Susceptibility of β -[(CH₃)₄N][Pd(dmit)₂]₂.

The close and open circles show the two independent data measured on the different samples. Arrows indicate the susceptibility maxima at 3 K.

range.^{14,15)}

5. Phase Diagram. As mentioned before, the general phase diagram of Bechgaard type organic conductors has been presented by Jerome, where the charge localization state, spin-Peierls phase, SDW phase, metallic phase, and superconducting region were located.¹⁰⁾ However the CDW state, which seems to play an important role in the DA₂ type M(dmit)₂ (M = Ni, Pd; D = TTF) superconductors, has no position in this phase diagram. Unlike DA₂ (or DA) type M(dmit)₂ superconductors, β -[(CH₃)₄N][Pd(dmit)₂]₂ is the 1:2 complex composed of closed-shell cations and π -acceptor molecules, Pd(dmit)₂. Besides the signs of the carrier and counter ion, the complex has the composition similar to that of Bechgaard salt. Furthermore, owing to the "HOMO-LUMO inversion", the dimensionality of the conduction band of β -[(CH₃)₄N][Pd(dmit)₂]₂ can be determined by the anisotropy of intermolecular overlap integrals of HOMO. Thus, it may be said from the view point of electronic structure that β -[(CH₃)₄N][Pd(dmit)₂]₂ belongs to the same class of conductors as the organic superconductors.

Based on the electric and magnetic properties described before, the phase diagram of β -[(CH₃)₄N][Pd(dmit)₂]₂ was determined. (1) At ambient pressure, the system is neither metallic nor semiconducting down to ca. 200 K, below which the resistivity increases gradually. It seems that the carriers tend to be localized with lowering temperature. But it is difficult to determine the critical temperature below which the system transforms to the semiconducting state. The ¹H NMR relaxation studies show that the AF (or SDW) phase transition takes place at 12 K. The amplitude of the magnetization was estimated to be 0.22 μ_B per Pd(dmit)₂ dimer.³⁰⁾ Although this amplitude is larger than the amplitude of 0.08 μ_B /TMTSF in Bechgaard salt,^{32,33)} the possibility of a simple AF order of localized moments was ruled out. And the 12 K transition was reported to be antiferromagnetic SDW transition.³⁰⁾ The susceptibility showed an additional anomaly around 3 K. (2)

With increasing pressure, the transition from highly conducting state to insulating state becomes sharp. At the same time, the transition temperature is decreased. (3) Around 4.5 kbar, the metal-insulator transition becomes clear and the transition temperature decreases very rapidly with increasing pressure. The ^1H NMR experiments show the SDW transition at 11 K, indicating that the SDW transition temperature is almost pressure independent between 1 bar and 4.5 kbar. (4) Above 5.3 kbar, a characteristic resistivity anomaly was observed around 60 K. But this anomaly is sample-dependent and not intrinsic. The metal-insulator transition appears below 30 K. A sharp resistivity decrease is observed at low temperature. The resistivity drop is suppressed by applying the magnetic field, which indicates that the onset temperature of the superconducting transition is somewhat higher than the offset temperature of the resistivity drop. (5) Above 7 kbar, the MI transition disappears and only the metal to superconductor transition is observed. The T_c decreases with increasing pressure and becomes zero around 9 kbar.

As shown schematically in the inset of Fig. 16, around 5.5 kbar the resistivity decreases very sharply with lowering temperature between T_{max} (the temperature where the resistivity takes a sharp maximum) and T_c (the superconducting temperature indicated by the complete resistivity drop). The temperature region between T_{max} and T_c can be regarded as the "pre-superconducting region," which can be found between 5 and 6.5 kbar. The maximum T_c of about 6.5 K is observed at the pressure where "pre-superconducting region" disappears.

Since the SDW transition temperature was found at 4.5 kbar and the "pre-superconducting region" exists above 5 kbar, the antiferromagnetic (or SDW) insulating phase seems to neighbor the superconducting phase. In this sense, the

phase diagram of $\beta\text{-}[(\text{CH}_3)_4\text{N}][\text{Pd}(\text{dmit})_2]_2$ seems to share a common feature with organic superconductors. Since the ^1H NMR studies showed that the rotational motion of methyl group is frozen around 120 K,³¹⁾ there seems to remain no freedom of the internal molecular motion at low temperature. As mentioned before, no indication of the structural phase transition was obtained by the low-temperature X-ray diffraction studies at ambient pressure. Since the crystal lattice will become more rigid with increasing pressure, the CDW transition with periodical lattice distortion will hardly be expected at high pressure.

In summary, $\beta\text{-}[(\text{CH}_3)_4\text{N}][\text{Pd}(\text{dmit})_2]_2$ is isomorphous to $[(\text{CH}_3)_4\text{N}][\text{Ni}(\text{dmit})_2]_2$, which is the first pure π acceptor conductor exhibiting the superconducting behavior at high pressure. The resistivity measurements revealed that the superconducting phase appears at 6–9 kbar. It may be interesting that the resistivity becomes very noisy at the pressure region where the system shows superconducting transition. The characteristic "pre-superconducting" region appears around 5.5 kbar. Similar to Bechgaard salt, the superconducting phase is located near the SDW insulating phase.

The authors would like to thank to Mr. H. Osako, Prof. A. E. Underhill, and Dr. R. A. Clark for their kind supply of the crystals and discussions. The low-temperature resistivity measurements under the magnetic field were made under the guidance of Profs. W. Sasaki, K. Kajita, and Y. Nishio, to whom our thanks are due. We are also grateful to Prof. T. Takahashi and Dr. Seya for the detailed information on the NMR studies.

References

- 1) D. Jerome, M. Mazaud, M. Ribault, and K. Bechgaard, *J. Phys. Lett.*, **41**, L95 (1980).
- 2) L. Brossard, M. Ribault, L. Valade, and P. Cassoux, *Physica B&C (Amsterdam)*, **143**, 378 (1986).
- 3) H. Tajima, M. Inokuchi, A. Kobayashi, T. Ohta, R. Kato, H. Kobayashi, and H. Kuroda, *Chem. Lett.*, **1993**, 1235.
- 4) A. Kobayashi, H. Kim, Y. Sasaki, R. Kato, H. Kobayashi, S. Moriyama, Y. Nishio, K. Kajita, and W. Sasaki, *Chem. Lett.*, **1987**, 1819; K. Kajita, Y. Nishio, S. Moriyama, R. Kato, H. Kobayashi, W. Sasaki, A. Kobayashi, H. Kim, and Y. Sasaki, *Solid State Commun.*, **65**, 361 (1988).
- 5) A. Kobayashi, H. Kobayashi, A. Miyamoto, R. Kato, R. A. Clark, and A. E. Underhill, *Chem. Lett.*, **1991**, 2163.
- 6) H. Kobayashi, K. Bun, T. Naito, R. Kato, and A. Kobayashi, *Chem. Lett.*, **1992**, 1909.
- 7) R. Kato, Y. Kashimura, S. Aonuma, N. Hanasaki, and H. Tajima, *Solid State Commun.*, in press.
- 8) K. Yamaji, *Solid State Commun.*, **61**, 413 (1987).
- 9) H. Kobayashi, A. Kobayashi, Y. Sasaki, G. Saito, and H. Inokuchi, *Chem. Lett.*, **1983**, 183.
- 10) D. Jerome, *Science*, **252**, 1509 (1991).
- 11) J. M. Williams, J. R. Ferraro, R. J. Thorn, K. D. Carlson, U. Geiser, H. H. Wang, A. M. Kini, and M.-H. Whangbo, "Organic Superconductors," Prentice-Hall, Englewood Cliff, NJ (1992).
- 12) K. Miyagawa, A. Kawamoto, Y. Nakazawa, and K. Kanoda,

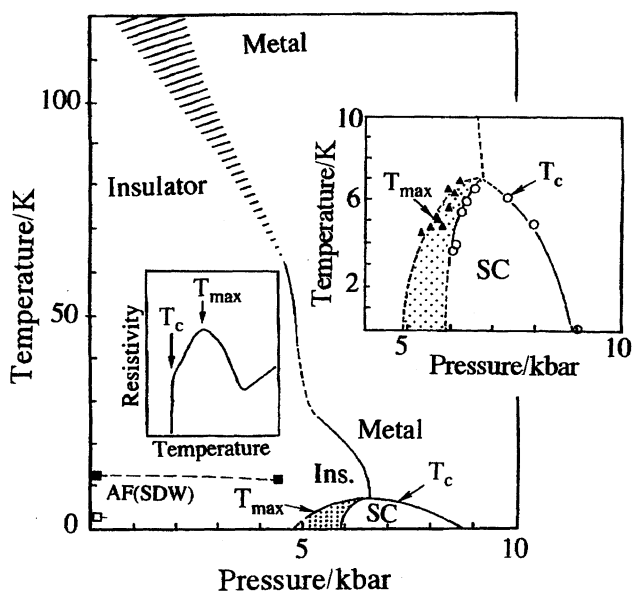


Fig. 16. Phase diagram of $\beta\text{-}[(\text{CH}_3)_4\text{N}][\text{Pd}(\text{dmit})_2]_2$.

The closed squares indicate the SDW transition temperature determined by ^1H NMR studies and the opened square is the temperature where the susceptibility shows a maximum.

Phys. Rev. Lett., **75**, 1174 (1995).

13) Y. Hasegawa and H. Fukuyama, *J. Phys. Soc. Jpn.*, **56**, 877 (1987).

14) A. Kawamoto, K. Miyagawa, Y. Nakazawa, and K. Kanoda, *Phys. Rev. Lett.*, **74**, 3455 (1995).

15) H. Mayaffre, P. Wzietek, D. Jerome, C. Leonoir, and P. Batail, *Phys. Rev. Lett.*, **75**, 4122 (1995).

16) H. Kobayashi, H. Akutsu, E. Arai, H. Tanaka, and A. Kobayashi, *Phys. Rev. B*, **B56**, R8526 (1997).

17) H. Seo and H. Fukuyama, *J. Phys. Soc. Jpn.*, in press.

18) P. Cassoux, L. Valade, H. Kobayashi, A. Kobayashi, R. A. Clark, and A. E. Underhill, *Coord. Chem. Rev.*, **110**, 115 (1991).

19) L. Brossard, M. Ribault, L. Valade, and P. Cassoux, *Phys. Rev. B*, **B42**, 3935 (1990).

20) G. Steinmecke, R. Kirmse, and E. Hoyer, *Z. Chem.*, **15**, 28 (1975).

21) A. Kobayashi, H. Kim, Y. Sasaki, K. Murata, R. Kato, and H. Kobayashi, *J. Chem. Soc., Faraday Trans.*, **86**, 361 (1990).

22) H. Osako, Master Thesis, Toho University (1992).

23) R. Kato, Y. Liu, S. Aomuma, and H. Sawa, *Solid State Commun.*, **98**, 1021 (1996).

24) T. Adachi, H. Kobayashi, and A. Kobayashi, to be published.

25) We have reported the crystal structure of α -[(CH₃)₂-(C₂H₅)₂N][Pd(dmit)₂]₂ (Ref. 6), where the different triclinic unit cell was adopted. In the previous lattice, the Pd(dmit)₂ molecules are stacked along [101].

26) E. Canadell, E. I. Rachidi, S. Ravy, J.-P. Pouget, L. Brossard,

and J. P. Legros, *J. Phys. (Paris)*, **50**, 2967 (1989); H. Tajima, M. Tamura, T. Naito, A. Kobayashi, H. Kuroda, R. Kato, H. Kobayashi, R. A. Clark, and A. E. Underhill, *Mol. Cryst. Liq. Cryst.*, **181**, 233 (1990); H. Tajima, T. Naito, M. Tamura, A. Takahashi, S. Toyoda, A. Kobayashi, H. Kuroda, R. Kato, H. Kobayashi, R. A. Clark, and A. E. Underhill, *Synth. Met.*, **41—43**, 2417 (1991); H. Tajima, T. Naito, M. Tamura, A. Kobayashi, H. Kuroda, R. Kato, H. Kobayashi, R. A. Clark, and A. E. Underhill, *Solid State Commun.*, **79**, 337 (1991).

27) A. Kobayashi, H. Kim, Y. Sasaki, R. Kato, and H. Kobayashi, *Solid State Commun.*, **62**, 57 (1987).

28) A. Kobayashi, H. Kim, Y. Sasaki, S. Moriyama, Y. Nishio, K. Kajita, W. Sasaki, R. Kato, and H. Kobayashi, *Synth. Met.*, **27**, B339 (1988).

29) M. Inokuchi, H. Tajima, T. Ohta, H. Kurada, A. Kobayashi, A. Sato, T. Naito, and H. Kobayashi, *J. Phys. Soc. Jpn.*, **65**, 538 (1996).

30) K. Seya, Y. Kobayashi, T. Nakamura, T. Takahashi, Y. Osako, H. Kobayashi, R. Kato, A. Kobayashi, and H. Iguchi, *Synth. Met.*, **70**, 1043 (1995).

31) T. Takahashi, private communications.

32) J. M. Delrieu, M. Roger, Z. Toffano, E. W. Milbogue, R. S. James, and K. Bechgaard, *Physica B+C (Amsterdam)*, **143B**, 412 (1986).

33) T. Takahashi, Y. Maniwa, H. Kawamura, and G. Saito, *Physica B+C (Amsterdam)*, **143B**, 417 (1986).